Measurement: Sensors 35 (2024) 101293

Contents lists available at ScienceDirect

Measurement: Sensors

journal homepage: www.sciencedirect.com/journal/measurement-sensors

On the utility of partially corrupted flow measurement data arising from adjacent acoustic Doppler current profilers for energy yield assessment

Luke Evans [a,b,*], Ian Ashton [c], Brian Sellar [d]

[a] EPSRC and NERC Centre for Doctoral Training in Offshore Renewable Energy (IDCORE), The University of Edinburgh, Exeter and Strathclyde, Grant Institute Kings Buildings, W Mains Rd, Edinburgh, EH9 3JW, UK
[b] European Marine Energy Centre (EMEC), Research Engineer, Orkney, The Charles Clouston Building ORIC, Back Rd, Stromness, KW16 3AW, UK
[c] University of Exeter, College of Engineering Mathematics and Physical Sciences, Penryn, Cornwall, UK
[d] The University of Edinburgh (UoE), School of Engineering, Edinburgh, UK

ARTICLE INFO

Keywords:
Acoustic Doppler profiler
Power performance assessment
Power curve
Tidal stream energy
Tidal turbine
Energy yield
Acoustic interference

ABSTRACT

Recommended practice for quantifying the energy resource at a tidal energy site requires the use of multiple instruments deployed across the site. However, the instruments used work by emitting an acoustic pulse and instruments working at the same time have the potential to interfere with each other through a process known as 'cross-talk'. It is important to understand the impact of cross-talk on measurements and how this can be managed and through data processing or suitable positioning of devices. The ReDAPT project conducted a measurement campaign using two Acoustic Doppler Current Profilers (ADCPs) placed upstream of an operational tidal turbine. This aimed to assess the 'in-line' instrument placement guidelines from IEC 62600-200 for Power Performance Assessment (PPA) in real-world conditions. Consequently, the results within hold potential to support arguments for expanding these zones or adjusting their general dimensions. Despite adhering to industry standards and best practices to eliminate unreliable data in the Quality Control (QC) checks, in both concurrently measuring ADCPs at different time stamps in approximately 15 % of the returned data. This work identified for the first time interference throughout the campaign and quantified subsequent impact on estimates. A method to remove data anomalies caused by interference between closely positioned ADCPs has been developed and demonstrated, resulting in a 7 % variation in estimated Annual Energy Production (AEP). The algorithm effectively removed approximately 90 % of the corrupted measurements. Moving forward, multi-sensor deployments could use the algorithm described to double-check for interference within the data sets, although care should be taken to avoid this by choosing a suitable layout for deployment.

Nomenclature

i	Index related to velocity bin
j	Index related to time stamp
L	Number of samples in the defined averaging period
n	Index related to data point
S	Number of depth bins across projected area of tidal energy converter
$\overline{P_i}$	Mean calculated tidal energy converter power in velocity bin i
$\overline{U}$	Mean power weighted rotor average velocity, m·s^{-1}
$\overline{u}$	Mean velocity, m·s^{-1}
$\widehat{U}$	Instantaneous power weighted rotor average velocity, m·s^{-1}
A	Type-A configuration, instrument location, A_1 and A_2
A_k	Depth bin over the swept area of the tidal energy converter, m^2
f_i	Proportion of time during an average year for which the mean current velocity occupies a value within velocity bin i

(*continued on next column*)

(*continued*)

N_B	Total number of velocity bins in the power curve
U	Mean velocity, m·s^{-1}
u	Velocity magnitude, m·s^{-1}
z	Height above seabed, m

1. Introduction

Tidal energy, a form of renewable energy, generates electricity from the cyclic rise and fall of ocean tides which are driven by interacting gravitational forces between the Earth, moon, and sun. Tidal energy produces minimal greenhouse gas emissions, thus aiding in reducing carbon footprints and combating climate change. To adopt tidal energy for a low-carbon future, a thorough understanding of the challenging

* Corresponding author. 3 Sunnybank Drive, Stromness, Orkney, KW16 3HS, UK.
E-mail address: Luke.evans@emec.org.uk (L. Evans).

https://doi.org/10.1016/j.measen.2024.101293
Received 30 August 2023; Received in revised form 11 August 2024; Accepted 13 August 2024
Available online 19 August 2024

ocean environment is crucial for efficient, cost-effective, and reliable tidal turbine systems [1]. To capture tidal flows, the commonly used acoustic Doppler current profiler (ADCP) remotely samples the water column over ranges/depths of tens to hundreds of meters without interfering with fluid flow [2–4]. ADCPs work by transmitting acoustic pulses into the water, which scatter off particles such as sediment and plankton. The transducers then receive the backscattered signals, and the frequency shift (Doppler shift) of these signals is analysed to determine water velocity [2–5].

ADCPs exhibit a range of configurations and transducer quantities, with the prevailing variant in the tidal industry being the four-beam divergent ADCP and its successor which includes an additional fifth-beam; a central vertically orientated transducer. These configurations allow us to capture different components of the water velocity vector. By combining data from multiple beams, we can reconstruct the three-dimensional velocity field. As the beam spread increases with the range from the instrument, sampling increasingly further away from the above-ADCP water column, it must be assumed that the flow is homogeneous between beams to determine flow profiles [2]. It is assumed that the velocity within each measurement cell (sample volume) along the profile is measured virtually simultaneously given the speed of sound in water (approximately 1500 m s^{-1}) relative to the speed of the sampled current. The beam path of each individual transducer is typically known as the *main lobe*. All transducers have a *side lobe* - a small amount of the transmitted energy falls outside the *main lobe* [6].

Instruments positioned near structures, cables, or other acoustic devices may encounter increased backscatter, not only from typical sources within the *main lobe* or *side lobe* regions but also from these adjacent objects [6], refer to Fig. 1. Such proximity can lead to signal contamination, distinct from cross-talk, which arises when the acoustic beams intersect fixed objects within their paths. This form of contamination often appears as horizontal lines in echogram representations, particularly if these objects remain static [2,6]. However, if these interfering objects move relative to the Doppler sonar, the resulting range of contamination can evolve over time. On the other hand, cross-talk specifically refers to interference between multiple sonar units, which typically manifests as diagonal lines in data visualisations due to variations in the internal clock speeds of the different units. Users must be vigilant and understand these potential complications to prevent biases in measurements, which can become evident as either reduced flow velocity or increased echo amplitude. In contour images that plot the relationship between time, depth, and variables like velocity or echo amplitude, these biases are often distinctly visible, helping to identify the nature and source of interference [7,8].

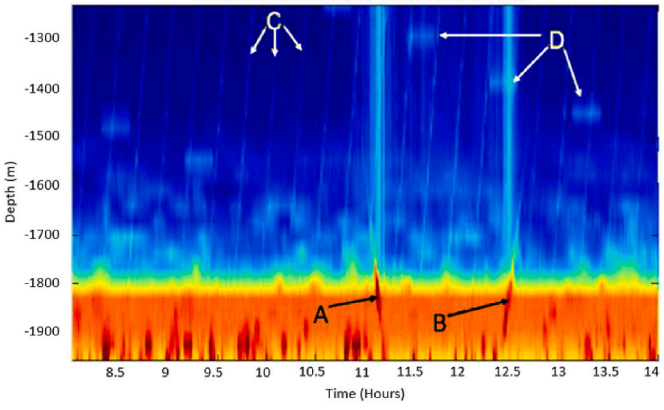

Fig. 1. Example of seabed mounted ADCP echo amplitude measurements featuring cross-talk characteristics, where A and B markers are strong vertical lines associated with the descent and ascent of a deployed remote-operated vehicle respectively. Markers C and D are diagonal and horizontal lines associated with cross-talk from other acoustic instruments [8].

Side lobe contamination from surface reflections and interference specific to a pair of ADCPs are distinct types of interference that affect ADCP data in different ways [9]. Side lobe contamination occurs when acoustic signals from an ADCP unit reflect off the water surface and return to the instrument, typically biasing the measured velocities to be lower than actual due to interference with the direct path signal, this has been comprehensively explored by Lentz, S.J [9]. The detection of this interference defines the extent of the contaminated surface region, which is influenced by factors such as water depth, beam angle, and bin size. It is crucial to note that this region has been excluded from the analysis, ensuring no overlap with the zone affected by cross-talk (interference specific to a pair of ADCPs). In contrast, cross-talk occurs when two units are deployed in close proximity and their acoustic signals interfere with each other. Cross-talk introduces erroneous data points and spikes, making velocity measurements unreliable. It is usually identified through comparative analysis between the two ADCPs, using methods like the spike test, a standardised test from the Quality Assurance of Real-Time Oceanographic Data (QARTOD), which is used to detect sudden, unexplained discrepancies.

Measurement campaigns must take into account the specific infrastructure that they are designed to measure. Numerous Tidal Energy Converter (TEC) designs exist and differ in characteristics like rated power, rated velocity, and deployment depths (z) in the water column. For floating turbines, assessing power performance becomes more complex due to motion from mooring cables and flow velocity variations in the upper water regions. Additionally, wind-induced flow and wave-current interaction further impact the floating TEC concepts of tidal flow variation. The removal of measured flow data near the surface can affect the calculation of the power-weighted rotor average (PWRA) velocity, a metric recommended in IEC TS 62600-200 [10]. Moreover, floating TEC concepts necessitate mooring systems that occupy the water column around the device, posing a challenge for ADCP placement. It becomes crucial to maintain a distance from potential cross-talk caused by the mooring system and device in the upper water column [6].

Within the Reliable Data Acquisition Platform for Tidal (ReDAPT) project [11], multiple ADCP deployments took place at the European Marine Energy Centre (EMEC) full-scale tidal test site at the Fall of Warness (FoW) between 2011 & 2015 (Fig. 2). The objectives were to evaluate flow characteristics and in-situ measurements for Alstom's DEEP-Gen IV 1 MW tidal turbines power performance. Recent studies indicate that spatial variations in current flow and direction significantly influence performance metrics [12,13]. One measurement campaign (out of seven) assessed the current flow variation upstream of the turbine using two concurrent flow sensors to comply with the guidelines set by the International Electrotechnical Commission (IEC) [12,14]. The IEC Technical Specification (IEC TS 62600-200) guides tidal developers in assessing machine performance [10]. According to this IEC TS, power performance should be measured relative to two independently located current profilers deployed in either 'in-line' (preferred) or 'adjacent' (least preferred) orientations at ranges based on the turbines diameter equivalent (D_E) [10].

This study investigates the impact of measurement cross-talk on the power performance assessment of an operational 1 MW tidal turbine and two modelled turbines. The analysis focuses on the effect of measurement bias on the power curve using in-situ data from two ADCPs located upstream on the flood tide of the DEEP-Gen IV at the Fall of Warness (Orkney, Scotland). This first-of-its-kind deployment at the site aimed to identify any near-machine upstream flow effects during the operation of the DEEP-Gen IV 1 MW tidal turbine and, on the alternate tide, wake effects. Despite passing the relevant QC checks outlined by QARTOD [15], this work identifies incidences of cross-talk between the two ADCPs, which would not be visible if adhering to the IEC 62600-200 (which requires a singular ADCP upstream of the TEC) by placing a second ADCP within 3 effective diameters of the first on the same side of the rotor.

However, this dataset is unique as it allows a review of data from two

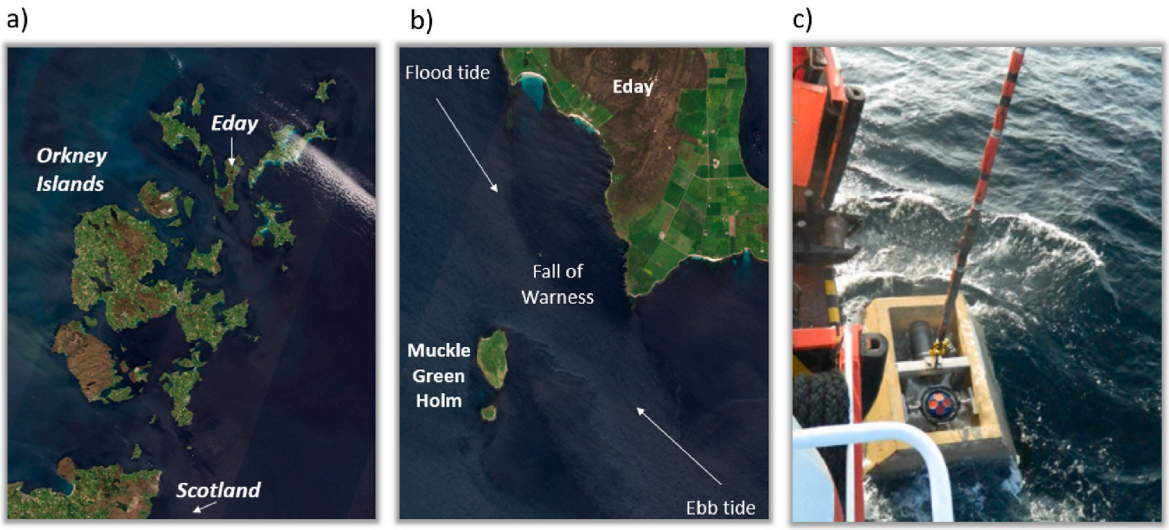

Fig. 2. Location of the study site. a) Orkney Islands location relative to Scotland; b) EMEC's full-scale tidal test site at the Fall of Warness, Eday; c) RDI ADCP in Gravity-based concrete frame being deployed. Image sourced from Ref. [11].

locations upstream of an operating turbine, enabling the conduction of two power performance assessments with more than 15 days of good data from both instruments, satisfying the IEC standard. Additionally, the study provides a robust method for removing interference from a dataset, offering valuable insights for deployments that encounter periods of interference and cannot afford to waste the collected data. This approach not only enhances the usability of contaminated datasets but also contributes to cost efficiency and knowledge transfer in ADCP deployments.

A methodology is proposed and demonstrated to identify and correct the interfered measurements, with a further study conducted to assess the impact of anomalous and filtered data on Annual Energy Production (AEP), a key techno-economic metric in the sector. Furthermore, the study addresses a key challenge of implementing IEC 62600-200 - deploying ADCPs within specified zones that are often small relative to water depth at deeper sites. The results advocate for expanding these zones or adjusting their dimensions.

The manuscript is structured as follows: Section 2 introduces the Fall of Warness tidal test site (Section 2.1), instrumentation relevant to this work (Section 2.2), turbine operational principles (Section 2.3), the modelled power for two other horizontal axis turbines (Section 2.4) and the power weighted rotor average method (Section 2.5). Section 3 outlines the methodology, the method for identifying the cross-talk (Section 3.1). The results are presented in Section 4, highlighting the difference between in-situ measurements between ADCPs (Section 4.1), impact on the power performance estimates (Section 4.2) and the variation in AEP estimates (Section 4.3) when data featured cross-talk characteristics. The results are discussed and concluded in Sections 5 and 6 respectively.

2. Test overview

2.1. Deployment site conditions

To ensure an obstacle-free environment, a rectangular area of 10 D_E x 20 D_E was surveyed for the power performance assessment (PPA) following IEC TS 62600-200 guidelines [10,12]. Fig. 3a depicts the survey area relative to the DEEP-Gen IV and the two ADCPs (known from here forward as A_1 and A_2 which are situated at 61 and 106 m

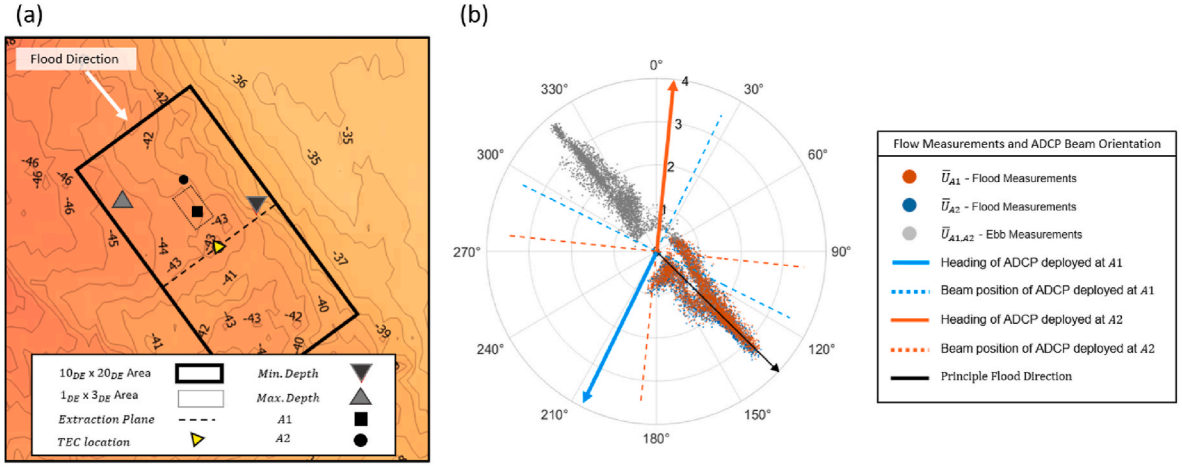

Fig. 3. Channel bathymetry and ADCP locations relative to the DEEP-Gen IV a t the FoW tidal test site. (a) The area of interest (solid black rectangle) showing the depth around the DEEP-Gen IV 'Contains Maritime and Coastguard Agency data © Crown Copyright' [16]. (b) Tidal ellipse for the flood tide PWRA flow velocities $\overline{U}_{A1}$ (orange dot) and $\overline{U}_{A2}$ (blue dot), with the beam orientation of both instruments (solid line representing main beam heading - beam 3 for RDI Work Horse (WH) ADCPs) and the principle flow direction is shown as the red line. Ebb data (grey) is not used in this analysis. Images adapted from [12,13].[12,13]. (For interpretation of the references to colour in this figure legend, the reader is referred to the Web version of this article.)

upstream of the DEEP-Gen IV respectively). For the purpose of a PPA the ADCP must be positioned within a rectangular area measuring 3 D_E long, 1 D_E wide and commencing at 2 D_E upstream of the turbine rotor. However, a significant challenge in implementing IEC 62600-200 has been effectively deploying ADCPs within the specified zones, particularly in deeper sites where these zones may be relatively small compared to the water depth. In this campaign, both ADCPs were deployed upstream of the turbine at distances of 3.4 D_E and 5.5 D_E exceeding the specified deployment zone outlined in IEC 62600-200.

The depth within this area varies from 46 m northwest of the turbine to 39 m near the east side. The typical flood tidal currents' directionality and strength at the deployment location are depicted in Fig. 3b. In a Janus configuration of a four-beam instrument like the Teledyne RDI ADCPs, the main heading is usually derived from the "forward-looking" beam. In this context, the ADCPs, labelled as A_1 and A_2, face approximately 206°and 6°, respectively. The forward-looking beam, oriented in the direction of the currents movement, serves as a crucial reference for determining the ADCPs' orientation relative to the flow direction and accurately calculating current velocities in various directions.

At this site, the flood tide reaches approximately 3.5 m s^{-1} with a direction offset of about 45° from the South. On the other hand, the ebb tide can reach up to 4 m s^{-1} and is known to feature higher turbulence, attributed to various features in the site bathymetry and nearby islands, as reported by others [17,18]. However, for this study, the ebb tide measurements were excluded since the instruments were placed in the wake of the TEC during this tide.

2.2. Instrumentation

Two RDI workhorse 600 kHz ADCPs (4 beams, 20-degree variant) were used, configured with 1 Hz sampling with a resolution of 1 m depth bins as specified in Table 1. Fig. 4 illustrates the displacement in the vertical and horizontal plane between the two deployed ADCPs A_1 and A_2 and the relative clearance zones (transparent cones around the transducers' main lobes). Instrument locations are specified in Table 2.

Fig. 5 illustrates a key scenario relevant to this study, involving two seabed ADCPs positioned 45 m apart. This figure shows how the signal from the source sensor spreads into the measurement column (vertical column that extends from the water surface to the seafloor). If the transducer beams of the two ADCPs are not perfectly aligned but remain relatively close, part of the signal pulse from the source sensor can reflect at an angle that matches the receiving ADCP's orientation. This misaligned reflection, interacting with the free-stream velocity component u, which causes an un-predictable pulse that arrives at the other co-located ADCP. This delay results in the second ADCP receiving the shifted signal later than expected, which introduces a measurement bias.

2.3. Turbine description

The operational TEC is a 1 MW rated machine featuring a traditional three-blade, horizontal axis design with an 18 m diameter rotor and variable-pitch control. The relevant turbine parameters are listed in Table 3. Throughout the study, this turbine will be referred to as TEC_{T2} (due to its position relative to the other two variants used in the analysis). To evaluate the impact of cross-talk on the measured power curve at different depths, two further variants of horizontal axis tidal turbines, which operate in different locations of the water column, were examined.

The designs of turbines TEC_{T1} and TEC_{T3} are based on deployed variants of horizontal-axis turbines. These designs were derived from the RealTide project [19], and their basic parameters are provided in Table 3.

Table 1
Instrument settings during the measurement campaign.

Specification	Unit	A_1 & A_2
Model		RDI WH 4 beam
Abbreviation		ADCP
Operating Frequency	kHz	600
Sample Rate	Hz	1
Cell Size	m	1
Beam Angle	°	20
Estimated Beam Width	°	2
Clearance Zone	°	11

2.4. Modelled power

The two separate power curves were created to simulate power production for the 0.1 MW and 2 MW TEC concepts. The power calculation method is illustrated by Equation (1):

$$P_{\text{active}} = P_{\text{rated}} \cdot \left(\frac{U^2 - U_{ci}^2}{U_r^2 - U_{ci}^2} \right) \tag{1}$$

here, P_{rated} represents the predefined rated power, U is the in-situ velocity measurement in m·s^{-1}, U_{ci} is the cut-in velocity for the proposed TEC, and U_r is the rated flow velocity for peak power production. Velocity measurements below the cut-in velocity are rejected, and those above the rated velocity are set to the defined rated power. This method is beneficial because it directly incorporates the turbine specific parameters, providing a straightforward and realistic estimation of power output across a range of current velocities, which is adequate for our comparison purposes. The quadratic model was chosen over the cubic model because it can provide a more conservative and realistic representation of tidal turbine power output, particularly at lower velocities, accounting for mechanical and environmental factors that may prevent immediate efficiency gains and thereby better capturing the gradual power increase from cut-in to rated speeds. Energy production was calculated using available time series power data from each instrument. This was achieved through the trapezoidal method, which approximates the power integral. The resulting energy was then scaled by the campaigns deployment ratio relative to the length of a year, as depicted in Equation (2):

$$AEP = R \cdot \Sigma_{t1}^{t2} \cdot \overline{P} dt \tag{2}$$

where AEP represents the anticipated annual energy production in MWh, R is the ratio of the number of days in a year to the deployment duration, $\overline{P}$ signifies the calculated mean TEC power, t_1 denotes the index number marking the beginning of the time interval, and t_2 indicates the index number marking the end of the time interval.

2.5. Power weighted rotor average velocity

To comply with the guidelines of IEC/TS 62600-200 [10], the current flow was averaged directly over depth bins that corresponded to the positions and diameters of three rotors in the water column, following the method of bins. To calculate the power-weighted rotor average (PWRA) velocity for the two seabed-placed ADCPs, the velocity measurements from depth bins corresponding to the rotor plane were averaged [13]:

$$\widehat{U}_{i,j,n} = \left[\frac{1}{A} \Sigma_{k=1}^{S} U_{i,j,k,n}^3 A_k \right]^{\frac{1}{3}} \tag{3}$$

where i represents the index number defining the velocity bin, j represents the index number of the time instant at which the measurement is performed, k represents the index number of the current profiler bin across the projected capture area, S is the total number of current profiler bins across the projected capture area, $\widehat{U}_{i,j,n}$ denotes the instantaneous power-weighted tidal current velocity across the projected capture area in m·s^{-1}, $U_{i,j,k,n}$ represents the magnitude of the instantaneous tidal current velocity for time j, at current profiler bin k, in

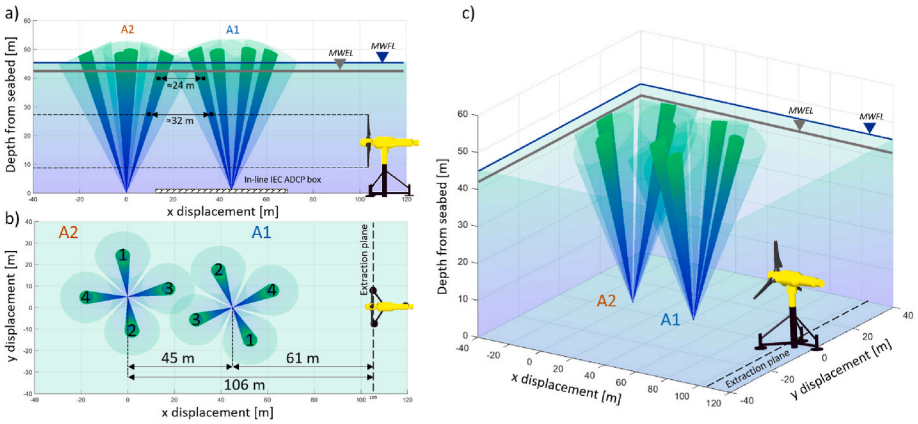

Fig. 4. RDI WH 600 kHz ADCPs, A_1 and A_2, which are 61 m and 106 m northeast of the TEC location (upstream on a flood tide), respectively. (a) Distance between neighboring beam trajectories from $ADCP_{A1}$ and $ADCP_{A2}$. Beam distance at the upper rotor bound (circle) and close to the sea surface (square) and the mean water level for the flood (blue triangle) and ebb (grey triangle). IEC TS 62600-200 instrument target box is included as the lined box. (b) Showcases the top-down view of A_1 and A_2 beam paths and the clearance zones. (c) Illustration of the main lobes (solid), clearance zones (shaded), and the orientation of the two bottom-mounted ADCPs. (For interpretation of the references to colour in this figure legend, the reader is referred to the Web version of this article.)

Table 2
Turbine proximal deployments of ADCPs showing unique campaign ID, date deployed (date format yyyy-mm-dd) and deployment duration. The coordinate system is in Decimal Degrees - WGS84.

ADCP ID	Campaign ID	Deployed	Recovered	Days	LN [°]	LW [°]
A_1	ADCP01-NWDep5	2014-06-22	2014-08-05	41	59.13726	2.80651
A_2	ADCP02-NWDep5	2014-07-07	2014-08-16	40	59.13764	2.80686

LN/LW: Location North/Location West

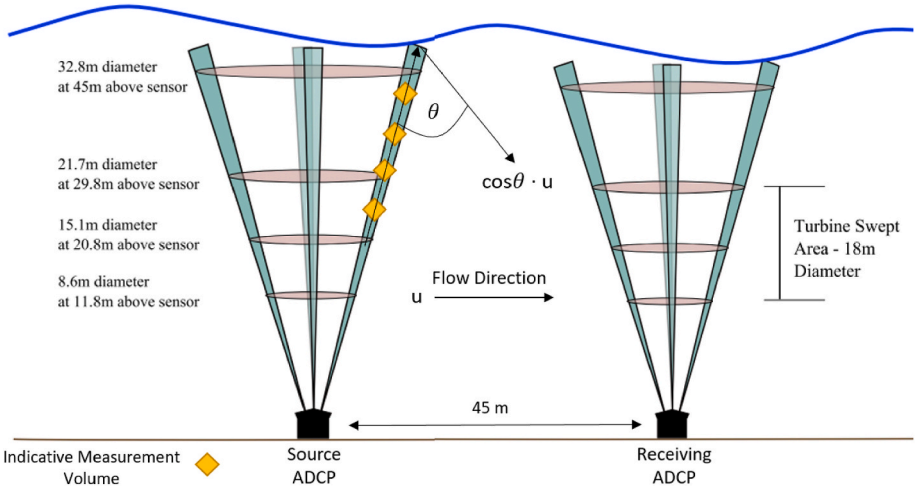

Fig. 5. Illustration of the theory of two angled sensors measuring a component of the free stream velocity along the angle intersecting the two beams. NOTE the rhombus volumes represent the ADCP weighting as per user manuals [2] where the depth cell is most sensitive to velocities at the centre of the cell.

Table 3
Key parameters of the DEEP-Gen IV TEC_{T2} and two further modelled variants, TEC_{T1} and TEC_{T3}.

Specification	Units	TEC_{T1}	TEC_{T2}	TEC_{T3}
Type	–	HATT	HATT	HATT
Distance above seabed	m	12	18	30
Blade radius	m	6	9	10
Projected capture area	m^2	113	256	314
Rated output power	MW	0.1	1	2
Cut-in	$m{\cdot}s^{-1}$	0.75	1	1.2
Rated speed	$m{\cdot}s^{-1}$	2.0	2.7	3.0

HATT: Horizontal-Axis Tidal Turbine.
NOTE: All turbines used in this study have 3 blades.

velocity bin i, for data point n in $m{\cdot}s^{-1}$, and A is the projected capture area of the proposed TEC in square meters.

The in-situ measurements were averaged by 5 min. Where $\widehat{U}_{i,j,n}$ should be averaged to calculate the mean PWRA velocity corresponding to the extraction plane of each rotor in the study. The averaging process is visually represented in Fig. 6 and expressed by Equation (4):

$$\overline{U}i,n = \left[\frac{1}{L}\sum_{j=1}^{L}\widehat{U}_{i,j,n}^{3}\right]^{\frac{1}{3}} \tag{4}$$

The measurements were grouped into velocity increments of 0.1 m s^{-1}, and the data within each bin were further averaged to obtain a single-point average. The study considers the PWRA velocity calculated

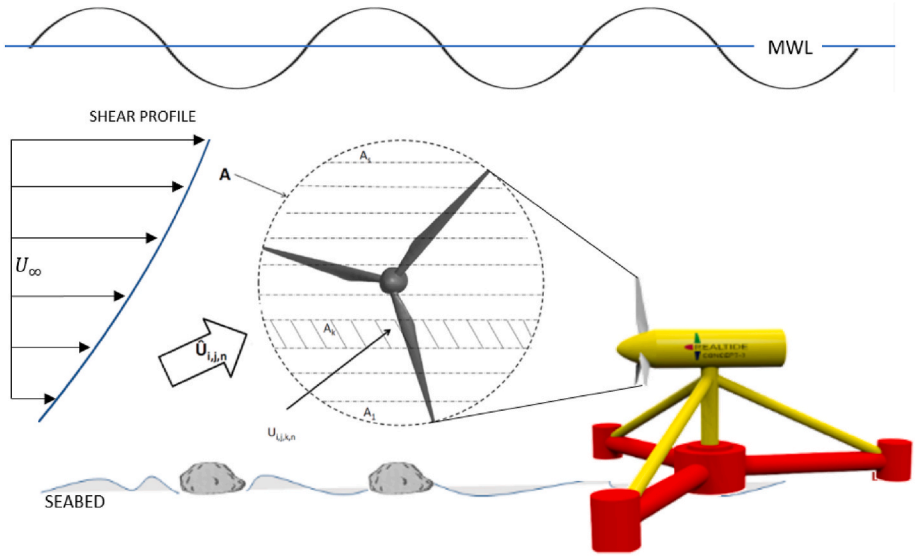

Fig. 6. The vertical variation of tidal current across the projected capture area - introducing the importance of the power PWRA technique. Image sourced from Ref. [13].

from instruments A_1 and A_2. For each turbine variant, the PWRA velocity from instrument A_1 is represented as $\overline{U}A_{1,T1}$, $\overline{U}A_{1,T2}$, and $\overline{U}A_{1,T3}$, while for instrument A_2, it is denoted as $\overline{U}A_{2,T1}$, $\overline{U}A_{2,T2}$, and $\overline{U}A_{2,T3}$.

3. Methodology

3.1. Identification and removal of the bias

Bias in ADCP measurements emerges as a consequence of the cross-talk between two instruments positioned in close proximity to each other. This cross-talk, often referred to as "acoustic interference," introduces distortions in the acquired data due to the overlap of acoustic signals emitted by one instrument and received by the other. The bias manifests as deviations from the true values, rendering the measurements susceptible to misinterpretation.

ADCP data typically undergoes rigorous quality checks to ensure that extreme outliers do not distort the analysis results. The QARTOD guidelines are highly recommended for quality control of ADCP data, as they provide both required and recommended checks, including setting appropriate thresholds. Key checks recommended by QARTOD guidelines that are relevant for detecting interference include the range test, which ensures data values are within expected ranges, and the flat line test, which identifies periods with no data variation. The spike test identifies data points that significantly deviate from the expected or neighboring values within a dataset, helping to detect and correct outliers or anomalies, while the attenuated signal test aims to flag issues with signal strength. Additionally, the surface echo test identifies interference from surface reflections. Together, these checks help mitigate the effects of interference and maintain the accuracy of the data analysis.

Table 4 provides a simple set of flags, as per guidance from QARTOD [15] - and associated descriptions that have been used in the data post-processing phase. For example, if the data failed the current speed test by exceeding the upper limit, a 'failed high' flag may indicate that the values were higher than the expected range.

Data anomalies passing through the quality control were then identified by the author as strong diagonal lines. This led to the development of an algorithm that could detect these features caused by acoustic cross-talk. The proposed method involves manipulating the data to locate the bias caused by cross-talk and disregard the corrupted measurements from further analysis.

To effectively identify cross-talk in echo amplitude profiles, data

Table 4
Assigning specific flags to data points that display potential anomalies or issues, helping to categorise and address the reliability of measurements, as per QARTOD.

Flag	ID	Description
Pass	1	Data have passed critical QC tests and are deemed adequate for use as preliminary data.
Not evaluated	2	Data has not been QC-tested, or the information on quality is not available.
Suspect or of high interest	3	Data are considered to be either suspect or of high interest to the user. They are flagged suspect to draw further attention to them.
Fail	4	Data are considered to have failed one (or more) critical QC check. If they are disseminated at all, it should be readily apparent that they are not of acceptable quality.
Missing data	9	Data are missing, used as a placeholder.

points were flagged for removal based on two key criteria: exceeding a prominence of 5 counts and containing two peaks in the detrended and smoothed amplitude profile. These conditions suggest potential acoustic cross-talk in this data set. Data with more than 5 counts but lacking two peaks were flagged, although not removed, due to limitations in the algorithms capacity to fully address complex cross-talk patterns near boundary layers. The algorithm assigns a flag of 4 to data that fail the check, indicating unacceptable quality. To quantify the total number of samples affected by cross-talk, the flagged data was summed for this quality control check and compared it to the overall data set.

The algorithm examines the contaminated averaged echo amplitude and time-averaged velocity profiles to identify peaks in echo amplitude. The cross-talk detection algorithm in amplitude performs the following tasks:

1. The 5-min averaged echo amplitude profiles are separated out individually to be assessed for indications of cross-talk.
2. The amplitude profile was detrended, subtracting the line of best fit (typically known as $y = mx + b$) from each profile.
3. The profile was then smoothed - using the function in MATLAB

(*smoothdata(X)*, where X is the dataset) a moving average filter of 3 data points was used - to remove small measurement fluctuations and distinguish the large peaks.

4. Finally, the profile is then multiplied by negative one to identify the primary peak (eliminating the peak found at the lower and most upper region of the water column due to boundary layers) to allow correct identification of the peak on either side of the biased measurement. The peaks were identified using the "findpeaks" function from the Curve Fitting Toolbox in MATLAB. The identified peaks had a prominence of at least 5 counts after detrending the data.

By removing the trend from the signal, the analysis focused on studying the significant fluctuations caused by cross-talk. The cross-talk consistently led to the identification of two peaks using this method. To address this, a set of quality control factors was introduced based on the number of peaks in the signal. The quality control factors and their corresponding flag as per QARTOD guidance are as follows:

- if $N_p <= 1$: flag data *1*;
- if $N_p = 2$: flag data *4* between the two peaks;
- if $N_p > 2$, the trough between the number of peaks is checked, and the peaks on either side of the largest trough are flagged *4*

where N_p is the number of peaks, measurements that have been flagged as containing cross-talk have been removed from the analysis. It should be noted that data flagged as 4 can also be reclassified as 3 and used for further analysis. By representing this reclassified data with a different colour or symbol, we can effectively compare the data set with and without the flagged data, providing a more detailed and nuanced analysis.

3.2. Alternative approaches to mitigating cross-talk

While the algorithm developed in this study effectively detects data contamination in the presented example (see section 3.3), it is important to recognise its limitations. Specifically, the algorithms performance may vary under different contamination scenarios, such as those involving more complex noise patterns or more frequent levels of interference at the boundary layers. Additionally, the current algorithm may not be robust against all types of data anomalies, potentially limiting its applicability in diverse environments.

Alternative approaches to mitigating cross-talk contamination include altering ping rates, using interleaved sampling schedules, and employing parent-child arrangements. Adjusting the ping rates of nearby instruments can minimise data collection overlap, thereby reducing cross-talk, but this method requires careful coordination and calibration, increasing deployment complexity. Interleaving sampling schedules to prevent multiple instruments from sampling simultaneously can also avoid cross-talk, though this comes at the cost of losing synchronous data, which may be crucial for certain analyses. Finally, connecting instruments in parent-child configurations ensures synchronised transmission and avoids cross-talk, yet this approach can complicate the deployment and maintenance of the instrument network.

Each of these alternative solutions introduces a different type of complexity to the deployment process. For instance, altering ping rates and using interleaved sampling schedules require precise timing mechanisms and thorough testing to ensure accuracy and reliability. On the other hand, parent-child arrangements necessitate additional hardware and coordination, which could be prohibitive in large-scale or resource-limited deployments.

3.3. Removal of cross-talk features

A robust flow velocity measurement is crucial for accurate performance assessments. The presence of contaminated data, which passed the QC steps outlined by industry standards and instrument manufacturers can have a significant impact on the measured power curve and AEP estimates. To address this issue, a method is proposed in Section 3.1 to identify and remove the contaminated measurements, this is shown visually in Fig. 7. The method involved manipulating the data to highlight the contaminated sections and applying a flag to exclude them from further analysis. By implementing this approach, the study can compare the consequence of filtered/unfiltered data used in the measured power curve and AEP estimates.

During post processing the data set it was apparent that cross-talk interference impacted only one instrument at a time, rather than both simultaneously. This finding suggests that the interference source alternated between the two instruments, complicating the identification of the exact cause. One hypothesis for this intermittency could be related to the synchronisation of the ADCPs. It is possible that the ADCPs experience slight variations in synchronisation over time due to clock drift. As a result, one ADCP may briefly slip in and out of sync with the other, causing intermittent periods of cross-talk interference. During these periods, the ADCP that is slightly out of sync may inadvertently "listen" shortly after the other, leading to the observed alternating pattern of interference affecting only one instrument at a time. Fig. 8 depicts the interference from the two ADCPs by the diagonal lines (velocity reduction along the depth profile) and also presents that only one ADCP is affected at a time. While variations in clock speeds between separate instruments are beyond the users control, and perfect alignment or minimal differences could reduce the ability to remove contamination, this scenario is highly unlikely.

As the currents measured at the two ADCP locations were often similar and interference typically affected only one instrument at a time, the impact of interference on calculating the AEP can be accurately assessed by replacing measurements affected by cross-talk with the corresponding clean measurements from the other instrument, thereby obtaining the best-case scenario to compare against. However, it is important to note that this replacement approach is only valid when the currents are sufficiently homogeneous, such that the two instruments measure the same currents when there is no cross-talk. This method may not be applicable in regions of strongly sheared flow, where significant differences in measurements between the instruments could occur.

4. Results

4.1. Cross-talk impact: inter-instrument measurements

Initially, cross-talk was identified through analysis of velocity time series plots, as shown in Fig. 9a, allowing for a direct comparison between the two ADCPs. Following identification, the methodology previously outlined in section 3 was employed to flag and subsequently remove the contaminated measurements. This approach proved effective in removing up to 90 % of the samples that were influenced by interference, see Fig. 9b. The remaining data that passed through were from regions close to boundary layers, where accurately locating a peak proved challenging.

Fig. 10a and b highlight the individual mean velocity and echo amplitude profiles (dark blue) with features of cross-talk being removed (light blue) and have passed through the algorithm. Fig. 11a, b, and 11c show the correlation of the measured flow velocities (U_{A1} and U_{A2}) across the rotor plane of TEC_{T1}, TEC_{T2} and TEC_{T3} respectively.

Table 5 provides a detailed summary of the total samples available, flagged, and removed during flood tides over a 26-day measurement period for two ADCPs. It highlights the number of samples impacted by interference and the subsequent removal percentages, emphasising the rigorous data processing steps taken to ensure only high-quality, time-stamp-matching samples were used in the final analysis.

Fig. 11 provides an observation that underscores at higher depth bins, where signal levels from the profiler in question decrease while contaminating signal levels remain unchanged, the impact of cross-talk becomes more pronounced. This phenomenon highlights the initiation of measurement cross-talk at shallower depths, gradually diminishing in intensity with increasing depth. The cross-talk affects the velocity between 1 m s^{-1} and 3 m s^{-1}. The power-weighted flow velocity is

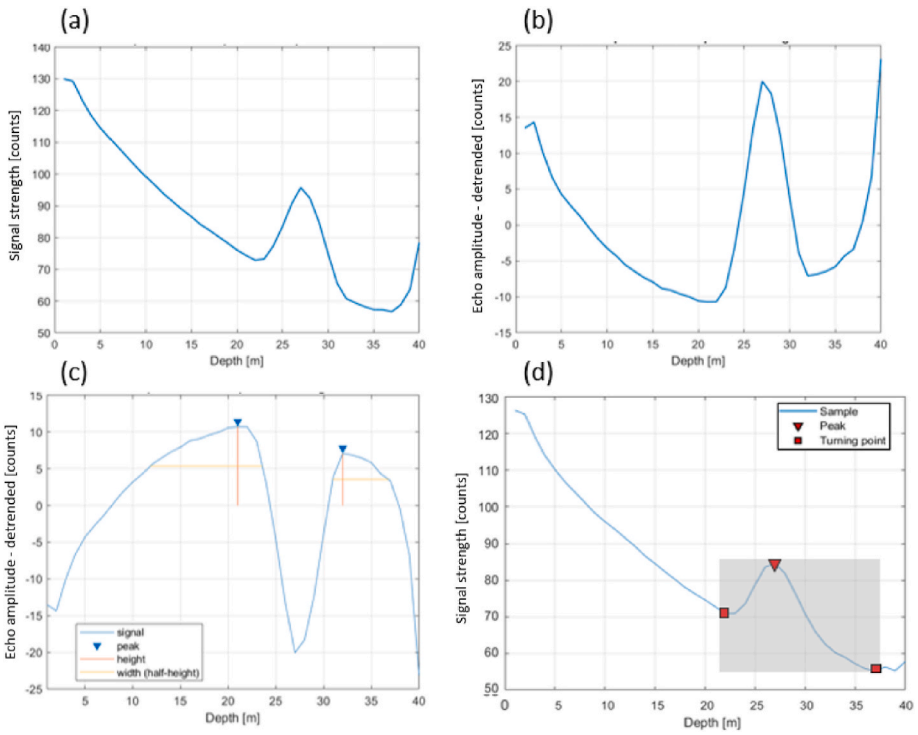

Fig. 7. Echo-Amplitude Depth Profile: (a) A data sample displaying a prominent peak in echo amplitude within the upper portion of the water column. (b) The amplitude profile detrended by subtracting the line of best fit. (c) The profile is then smoothed to remove multiple mini-peaks and then multiplied by negative one to identify the primary peak. (d) The algorithm effectively identifies the peak (indicated by a triangle) within the data sample, while also eliminating measurements between the designated square markers that represent bias from cross-talk features.

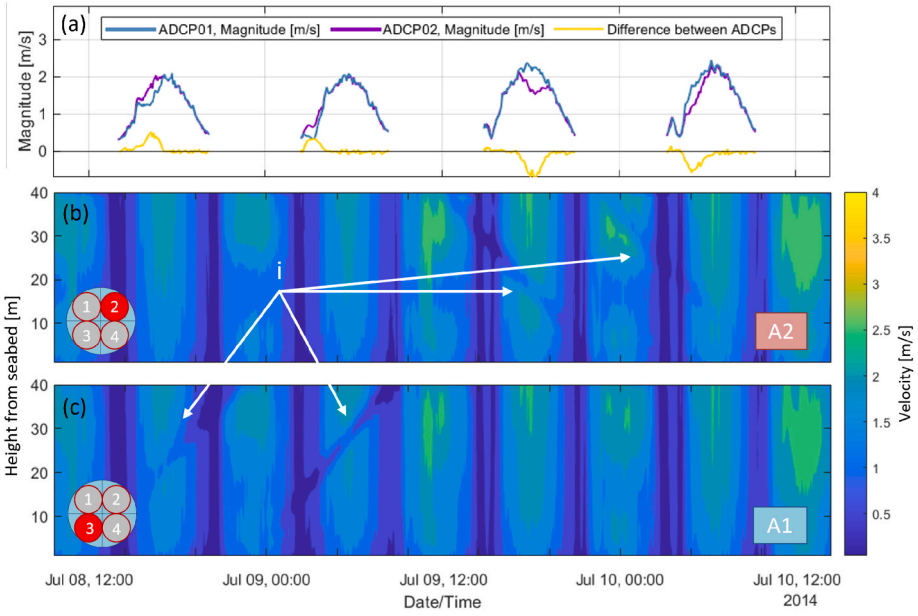

Fig. 8. (a) Velocity magnitude for A_1 (blue) and A_2 (purple) over four flood cycles, included is the difference between both velocity measurements (yellow). (b) Velocity depth contour for A_2 beam 2 (as depicted in the bottom left) where interference is identified as *i* - a diagonal line - for ADCP A_2. (c) Velocity depth contour for ADCP A_1 beam 3. (For interpretation of the references to colour in this figure legend, the reader is referred to the Web version of this article.)

compared, including periods of cross-talk across the depth bins used in the power-weighted calculation. The linear model coefficients (with 95 % confidence bounds) and the sum of squared error (SSE) are presented in Table 6. Where $z_{T\ldots}$ is representative of the bin depths used across the rotor diameter of TEC_{T1}, TEC_{T2} and TEC_{T3}. Also presented in Table 6 P1 and P2, these statistics represent correlation parameters between concurrently measuring ADCPs at A_1 and A_2. P1 assesses the alignment in magnitude of the measurements, while P2 evaluates the bias between them. These statistics are crucial for determining the agreement between the ADCPs.

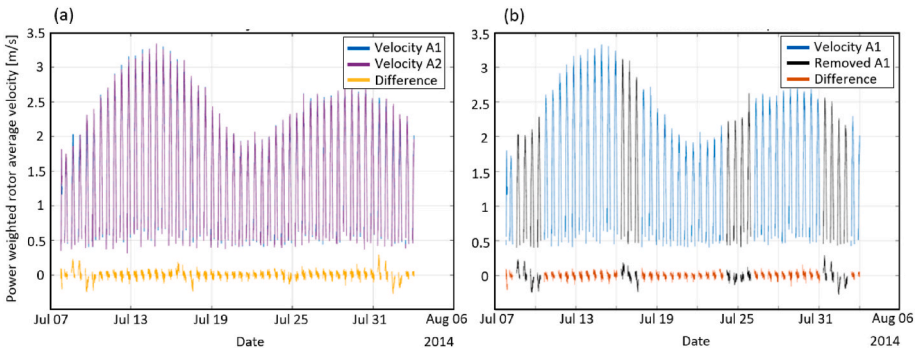

Fig. 9. (a) Time series comparison of power-weighted rotor average velocities from ADCPs A_1 and A_2, focusing on the TEC_{T2} rotor. The yellow line represents the difference between the two measurements. (b) Power-weighted rotor average velocity time series from ADCP A_1, highlighting flagged data influenced by interference (black line). The difference between ADCP A_1 and A_2 measurements is also depicted. (For interpretation of the references to colour in this figure legend, the reader is referred to the Web version of this article.)

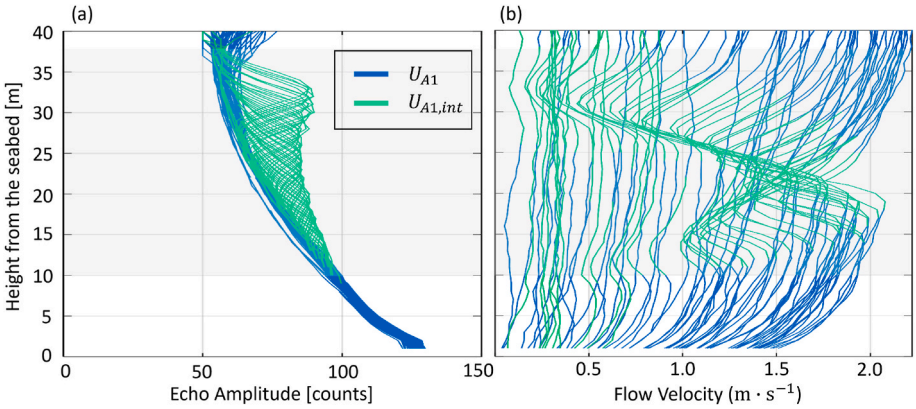

Fig. 10. An area of cross-talk is identified and highlighted in the grey box, and the good measurements (U_{A1}) and flagged contaminated measurements ($U_{A1,int}$) are given for one flood cycle. (a) Mean echo amplitude measurements in counts. (b) Mean flow velocity profile in m·s^{-1}.

4.2. Cross-talk impact: estimates of power performance

The main objective of this investigation is to analyze the impact of cross-talk on velocity measurements and its subsequent effect on estimated power metrics for a turbine. Fig. 12 presents three consecutive flood cycles, showing the varying locations of cross-talk along the water column (dashed lines), followed by three consecutive flood cycles with no cross-talk (solid lines). The PWRA velocity is calculated for measurements obtained across the swept area of three turbines represented by square, triangle, and circle symbols, corresponding to TEC_{T3}, TEC_{T2}, and TEC_{T1}, respectively.

In Fig. 13a, the generated power output for each 5-min measurement is plotted against the flood tide velocity component approaching the DEEP-Gen IV, TEC_{T2}. The flow velocity measurements containing cross-talk features are represented by blue dots, showcasing the variation caused by cross-talk between the two ADCPs. Additionally, the flow velocity measurements with 90 % of the cross-talk features removed are displayed as orange dots.

Fig. 13b illustrates the variation in the mean PWRA velocity (black dashed line) for measurements with and without cross-talk features. The PWRA velocity represents measurements taken across z_{T2}, the swept area of TEC_{T2}. At lower flow velocities, more noticeable differences are observed between the curves in Fig. 13b. The velocity differences range from 0.5 % to 2.5 % between flow velocities of 1–1.5 m s^{-1} and 1.5–2.0 m s^{-1} (where cross-talk occurs during the depth bins used for PWRA velocity calculation), respectively.

Had the cross-talk not been identified and removed, the power curve would shift to the left, favouring lower flow velocities when paired with the power produced by the DEEP-Gen IV. In the measurement campaign, 15 % of the flood tide data displayed significant interference features throughout the water column. The variation in flow velocity changes with depth, implying that the cross-talks impact on the measured power curve could be more significant depending on the depth bins used.

This effect becomes more evident when examining Fig. 14, where depth bins relative to the swept area of TEC_{T3} in the upper region of the water column (z_{T3}) are used. In this case, the cross-talk features are more pronounced, leading to a significant reduction in the measured velocity (as shown in Fig. 12).

The flow velocity, including the 15 % contaminated flood cycles, when used to generate the power curve, was found to be, on average, approximately 6 % lower than data unaffected by cross-talk. Neglecting to identify and remove these cross-talk features during the data post-processing phase can alter the power curve for the turbine under performance review, potentially misrepresenting the annual energy estimate. Hence, it is crucial to address cross-talk issues to ensure accurate and reliable turbine performance assessments.

4.3. Cross-talk impact: estimates of annual energy production

Using the velocity time series from ADCPs positioned at A_1 and A_2, along with the power produced by TEC_{T2}, the AEP can be calculated. During periods of cross-talk (which occurred in one instrument at any given time), the other instrument was used to estimate the AEP, allowing the impact of cross-talk to be quantified.

Considering the cross-talk affected approximately 15 % of the flood cycles, the results revealed a difference in AEP estimates of up to 4 %. The variability in AEP differences was observed when using different depth bins as the reference. The cross-talk effect on velocity

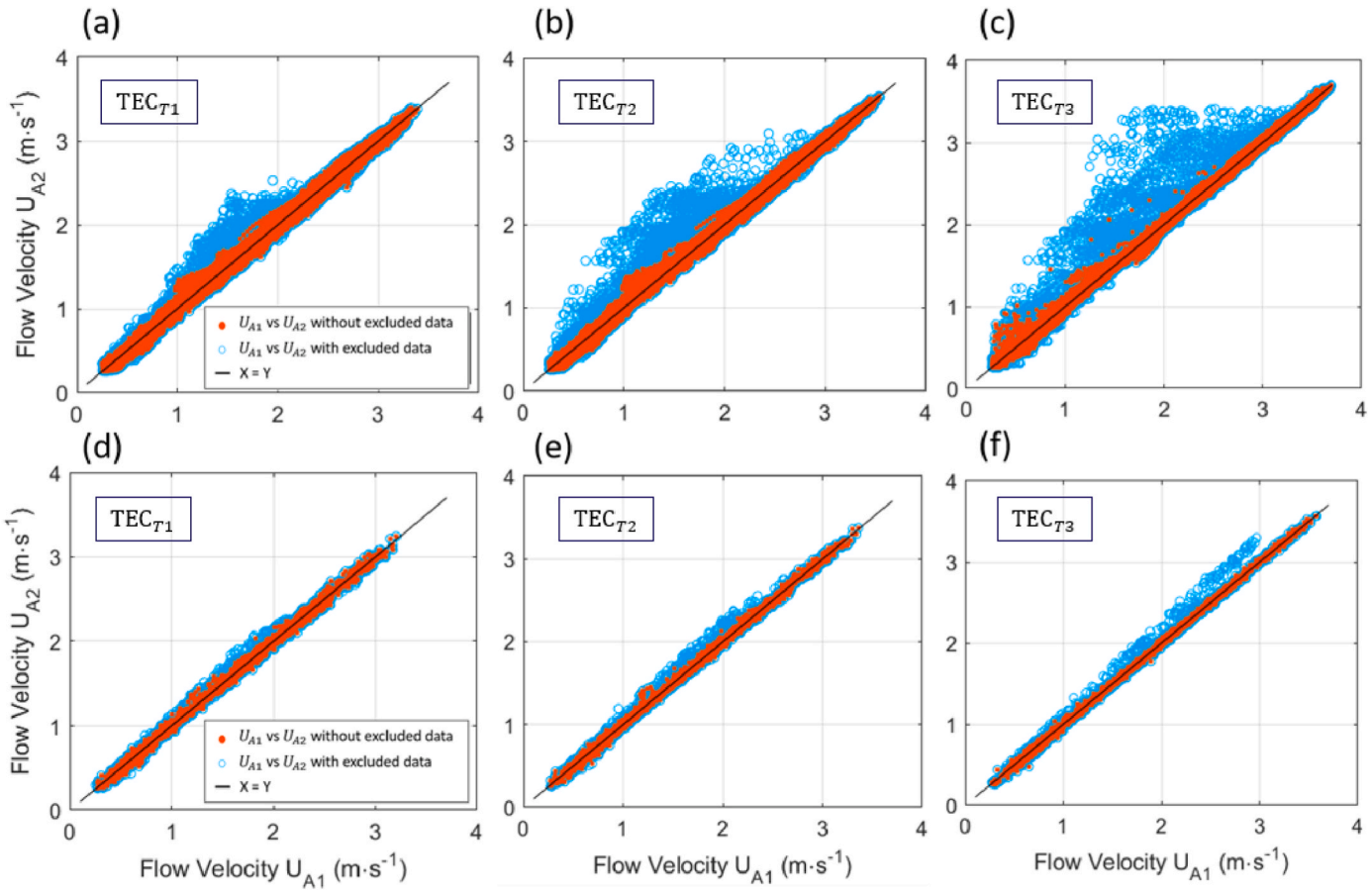

Fig. 11. Measurement correlation between flow velocities across the swept area of TEC_{T1}, TEC_{T2} and TEC_{T3} displayed in (a), (b) and (c) respectively, for data with (blue) and without (orange) features of cross-talk. PWRA velocity correlation across the swept area of TEC_{T1}, TEC_{T2} and TEC_{T3} illustrated in (d), (e) and (f) for data with (blue) and without (orange) features of cross-talk respectively. Perfect correlation illustrated as x = y (black line). (For interpretation of the references to colour in this figure legend, the reader is referred to the Web version of this article.)

Table 5
Overview of total samples available, flagged, and removed during flood tides over a 26-day (days of overlap between the co-located ADCPs) measurement period. Note that only samples with matching timestamps were included in the analysis for comparison. The table summarises the total number of samples.

ADCP ID	A_1	A_2
No. 5 min samples	3744	3801
No. interfered samples	562	646
No. samples removed	507	588
% removed	90.2	91.0
No. remaining 5 min samples	3237	3213
No. samples used in analysis	3213	3213

measurements was more significant in the upper region (z_{T3}) of the water column, resulting in differences in AEP of up to approximately 7 %. In contrast, the lowest difference in AEP with and without cross-talk features was found in the lower region of the water column (z_{T1}), where the difference was 2 %.

When cross-talk interference was absent, the measurements obtained at the two ADCP locations exhibited a high degree of similarity. This finding suggests the possibility of advocating for the expansion of these zones or the adjustment of their general dimensions, potentially by an additional 0.5 D_E, to accommodate more reliable data collection.

5. Discussion

In previous studies containing multiple acoustic velocity sensors, features of interference within the in-situ measurements were found to negatively affect the accuracy of velocity measurements. This study demonstrated that two ADCPs when placed close to each other (around 45 m apart), can still provide useful measurements. Nonetheless, this work identified for the first time interference throughout the campaign and quantified subsequent impact on AEP estimates. This interference was most pronounced at a certain range, where the possibility of the two

Table 6
Correlation parameters between concurrently measuring ADCPs located at A_1 and A_2. Velocities representative of the depth bins across the swept area of TEC_{T1}, TEC_{T2} and TEC_{T3} given by (a, d), (b, e) and (c, f) respectively. Correlation between PWRA velocities - calculated using depth bins across TEC_{T1}, TEC_{T2} and TEC_{T3} - with (a, b, c) and without (d, e, f) features of cross-talk are provided.

	Statistics	z_{T1}	z_{T2}	z_{T3}
U_{A1} vs U_{A2}		(a)	(b)	(c)
	P1	0.996	0.999	0.998
	P2	0.009	0.003	−0.007
	SSE	663	223	1465
	R^2	0.983	0.990	0.972
	RMSE	0.065	0.067	0.134
$\overline{U}_{A1}$ vs $\overline{U}_{A2}$		(d)	(e)	(f)
	P1	1.002	1.002	1.006
	P2	−0.005	−0.005	−0.020
	SSE	14.272	10.331	24.853
	R^2	0.993	0.994	0.991
	RMSE	0.061	0.052	0.081

z: depth across swept area.

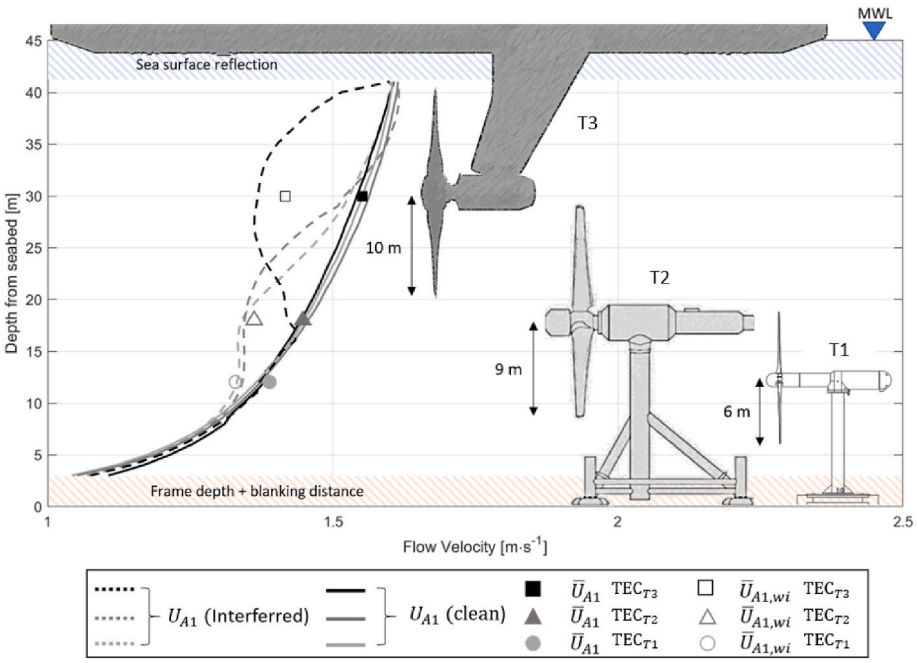

Fig. 12. Six consecutive flood tide depth profiles featuring cross-talk effects (dashed lines) and *clean* profiles (solid lines). The position of three variants of TECs are overlaid (*T*1, *T*2, and *T*3, at hub height 12, 18 and 30 m, respectively) with symbols showing corresponding interfered (unfilled) and *clean* (filled) PWRA velocities.

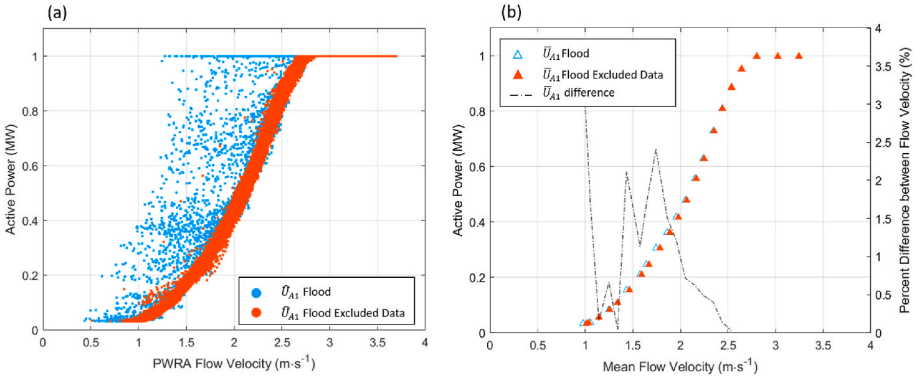

Fig. 13. The effect of ADCP cross-talk on the measured power curve - for TEC_{T2} - for the averaged 5-min PWRA velocities in increments of 0.1 m s^{-1}. (a) The flood tide measurements for ADCP A_1 ($\widehat{U}_{A1}$) with features of cross-talk (blue dot) from interacting with ADCP A_2, the orange dot represents data with cross-talk features removed. (b) The mean PWRA velocity from ADCP A_1 ($\overline{U}_{A1}$) with (blue triangle) and without (orange triangle) features of cross-talk in the 5-min averaged measurements. (For interpretation of the references to colour in this figure legend, the reader is referred to the Web version of this article.)

ADCPs picking up signals reflecting off the sea surface was greater. This interference seemed to be associated with one sensor at a time, making it difficult to pinpoint the exact cause.

Despite the interference, we managed to obtain data valid (≈80 % of the campaign) for the purpose of a power performance assessment. This work suggests that It's is possible to position two ADCPs on the seabed for vertical profiling at a depth of 45 m, separated by 45 m, and obtain reliable results. Notably, the interference caused a frequent shift in the location of peak interference (measurements corrupted between 10 and 40 m from the seabed), with the most significant impact occurring in the upper part of the water column (over 25 m from the seabed). This led to a bias in the measurements, where the velocity data is reduced, but still appreciable, at points where interference was strong.

The interference primarily affects current velocity in the range of 1–3 m s^{-1} – a range crucial for applications like tidal energy. Since the interference happened at various depths simultaneously, it greatly distorted the calculation of the PWRA velocity. This bias in the PWRA velocity, when combined with the generated power from the TEC, was observed to lead to a misrepresentation of up to 8 % at velocities directly relevant to turbine operation. These findings highlight the significance of eliminating data that distorts the representation of flow characteristics. This observation is particularly relevant in the context of a data campaign in which 15 % of the data was compromised. In scenarios where this level of corruption is greater, the consequences would be even more substantial.

A method to remove data anomalies caused by interference between these closely positioned ADCPs has been developed and demonstrated, resulting in a 7 % variation in estimated AEP. The method involved data manipulation that successfully removed interference features with an accuracy of up to 90 %. However, addressing interference in the uppermost region proved to be more intricate, primarily due to the heightened variability in velocity measurements.

6. Conclusion

This study introduces a novel perspective on the deployment of

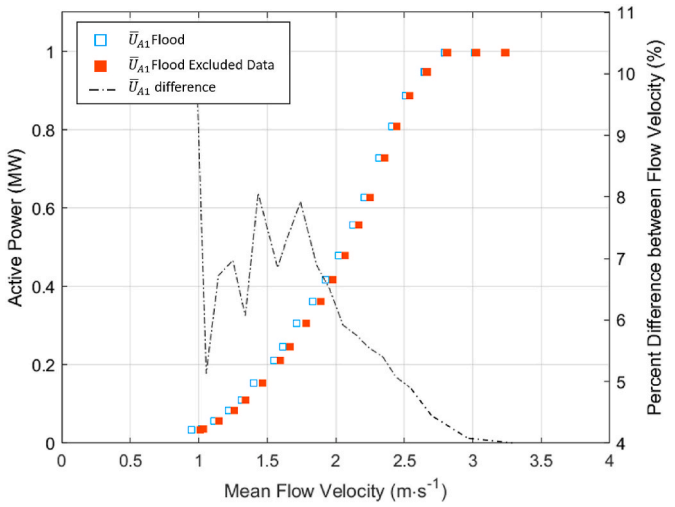

Fig. 14. The mean PWRA velocity from ADCP A_1 ($\overline{U}_{A1}$) with (blue square) and without (orange square) features of cross-talk in the 5-min averaged measurements across the rotor span of TEC_{T3}(z_{T3}). (For interpretation of the references to colour in this figure legend, the reader is referred to the Web version of this article.)

closely positioned ADCPs, demonstrating that two ADCPs placed 45 m apart can still provide valuable measurements, despite the challenges of interference (a consequence of not adhering to IEC 62600-200). For the first time, interference throughout the ReDAPT campaign was identified and quantified, revealing its significant impact on AEP estimates. The interference was most pronounced between 10 and 40 m from the seabed, affecting current velocities in the crucial range of 1–3 m/s for tidal energy applications.

Despite the interference, approximately 80 % of the data collected was valid and sufficient for accurate power performance assessment. This suggests that positioning two ADCPs 45 m apart on the seabed is viable for effective vertical profiling at a depth of 45 m. However, the interference introduced a bias in PWRA velocity calculations, leading to up to an 8 % distortion in velocities relevant to turbine operation.

To address this challenge, a method was developed to remove data anomalies with 90 % accuracy, resulting in only a 7 % variation in estimated AEP. This study underscores the importance of effective interference management and robust data cleaning techniques to ensure reliable turbine performance assessment and energy production estimates. These findings provide valuable insights for future research and practical applications, emphasising the need for accurate data in the context of tidal energy and other marine environments.

Against the backdrop of potential uncertainties, our findings highlight the resilience of the deployed ADCPs in capturing valid data for a PPA, despite interference. However, it is essential to recognise that the interference introduced a bias in PWRA velocity calculations, leading to up to an 8 % distortion in velocities directly relevant to turbine operation. Moreover, the resultant 7 % variation in estimated AEP underscores the importance of accounting for and mitigating the effects of interference in order to ensure accurate AEP estimates. By acknowledging these potential sources of uncertainty and their implications, our study contributes to a more comprehensive understanding of the challenges and opportunities in AEP estimation under real-world environmental conditions.

Data availability

To address the objectives of this project, in-situ data was required. Data from the ReDAPT project was chosen as a rich data resource (with unique multi-sensor deployments at a tidal energy site) that was available through the ReDAPT data exchange [20].

Author contributions

Luke Evans: Conceptualisation, Methodology, Formal analysis, Investigation, Writing – original draft, revision. Ian Ashton: Supervision and writing - review. Brian Sellar: Conceptualisation, Supervision, Writing – review.

Declaration of competing interest

The authors declare that they have no known competing financial interests or personal relationships that could have appeared to influence the work reported in this paper.

Data availability

Data will be made available on request.

Acknowledgments

The author gratefully acknowledges funding support from EPSRC and NERC for the Industrial CDT in Offshore Renewable Energy (IDCORE) (EP/S023933/1) and sponsorship by EMEC.

Abbreviations The following abbreviations are used in this manuscript:

TEC	Tidal Energy Converter
ADCP	Acoustic Doppler Current Profiler
PPA	Power Performance Assessment
AEP	Annual Energy Production
EMEC	European Marine Energy Centre
FoW	Fall of Warness
ReDAPT	Reliable Data Acquisition Platform for Tidal
DE	Equivalent Diameter
QC	Quality Control
PWRA	Power Weighted Rotor Average
QARTOD	Real-Time Quality Control of Stream Flow Observations

References

[1] M. J. Kreitmair, Uncertainty Quantification in Tidal Energy Resource Assessment.

[2] R.D.I. Teledyne, Acoustic Doppler Current Profiler: Principles of Operation, a Practical Primer, 2011, p. 56. P/N 951-6069-00. 00 (January), https://www.comm-tec.com/Docs/Manuali/RDI/BBPRIME.pdf.

[3] Nortek Manuals, Signature manual: principles of operation, Tech. rep. (2018). URL, https://www.nortekgroup.com/assets/software/N3015-011-SignaturePrinciples.pdf.
[4] Nortek Manuals, The comprehensive manual for ADCPs, J. Chem. Inf. Model. 53 (9) (2019) 1689–1699, https://doi.org/10.1017/CBO9781107415324.004.
[5] R.D.I. Teledyne, ADCP Coordinate Transformation, Formulas and Calculations 00 (July), 1997, p. 26. URL, www.rdinstruments.com.
[6] R.D.I. Teledyne, RD Instruments acoustic Doppler current profilers application: note ADCP beam clearance area, Tech. rep. (2002). URL, http://www.teledynemarine.com/Documents/BrandSupport/RDINSTRUMENTS/TechnicalResources/TechnicalNotes/ChannelMaster/FSA019.PDF.
[7] M. Jourdain De Thieulloy, M. Dorward, C. Old, R. Gabl, T. Davey, D.M. Ingram, B. G. Sellar, Single-beam acoustic Doppler profiler and co-located acoustic Doppler velocimeter flow velocity data, MD: Data 5 (3) (2020) 1–11, https://doi.org/10.3390/data5030061.
[8] J. Mullison, D. Symonds, ADCP Deployments Near Offshore Structures, Oceans Conference Record (IEEE)doi:10.1109/OCEANS.2007.4449258.
[9] R.D.I. Teledyne, A note on the depth of sidelobe contamination in acoustic Doppler current profiles, J. Atmos. Ocean. Technol. 00 (July) (2022) 31–35, https://doi.org/10.1175/jtech-d-21-0075.1.
[10] International Electrotechnical Commission (IEC), PD IEC/TS 62600-200 : 2013 BSI Standards Publication Marine Energy — Wave , Tidal and Other Water Current Converters Energy Converters — Power Performance.
[11] B. Sellar, D.R. Sutherland, Tidal energy site characterisation at the fall of warness , EMEC , UK energy technologies institute (ETI) ReDAPT MA1001 (MD3.8 release v4.0), Tech. rep. (2016) available at: http://redapt.eng.ed.ac.uk.
[12] L. Evans, I. Ashton, B. Sellar, Tidal turbine power performance assessments following IEC TS 62600-200 using measured and modelled power outputs, Renew. Energy 212 (2023) 138–150, https://doi.org/10.1016/j.renene.2023.05.031. URL, https://linkinghub.elsevier.com/retrieve/pii/S0960148123006547.
[13] L. Evans, I. Ashton, B.G. Sellar, Impact on energy yield of varying turbine designs under conditions of misalignment to the current flow, Energies 16 (9) (2023) 3923, https://doi.org/10.3390/en16093923. URL, https://www.mdpi.com/1996-1073/16/9/3923.
[14] J. Mcnaughton, R. Sinclair, B. Sellar, Measuring and modelling the power curve of a commercial-scale tidal turbine, Proceedings of the 11th European Wave and Tidal Energy Conference (October). doi:10.1017/CBO9781107415324.004. URL https://www.researchgate.net/publication/282327696.
[15] Integrated Ocean Observing System (IOOS), Manual for Real-Time Quality Control of Stream Flow Observations (QARTOD) v2.1 (July). doi:10.25923/sqe9-e310.
[16] Maritime, C. Agency, Guide to using the CHP Bathy Atlas. URL https://assets.publishing.service.gov.uk/government/uploads/system/uploads/attachment_data/file/296198/chp_bathy_atlas_guide.pdf.
[17] I. Afgan, J. McNaughton, S. Rolfo, D.D. Apsley, T. Stallard, P. Stansby, Turbulent flow and loading on a tidal stream turbine by LES and RANS, Int. J. Heat Fluid Flow 43 (2013) 96–108, https://doi.org/10.1016/j.ijheatfluidflow.2013.03.010.
[18] M. Lewis, J. McNaughton, C. Márquez-Dominguez, G. Todeschini, M. Togneri, I. Masters, M. Allmark, T. Stallard, S. Neill, A. Goward-Brown, P. Robins, Power variability of tidal-stream energy and implications for electricity supply, Energy 183 (2019) 1061–1074, https://doi.org/10.1016/j.energy.2019.06.181.
[19] RealTide Bureau Veritas, Advanced monitoring, simulation and control of tidal devices in unsteady, highly turbulent realistic tide environments, H2020 Programme for Research and Innovation 727689 (2019) 1–45. URL, https://www.realtide.eu/.
[20] B. Sellar, C. Old, D. Ingram, Dataset: field-measurements aligned to the implementation of a tidal energy converter's power performance assessment (IEC 62600-200 PPA Type B). https://doi.org/10.3390/en11010176, 2022.

Correspond author: Luke Evans will handle correspondence at all stages of refereeing and publication, also post-publication.